

AD-A061 801

NAVAL RESEARCH LAB WASHINGTON D C
FAILURE STUDIES OF A THIRD STAGE FAN DISK FROM A TF-30 TURBINE --ETC(U)
NOV 78 W H VAUGHAN, R J SANFORD, J M KRAFFT

F/6 21/5

UNCLASSIFIED

NRL-MR-3874

NL

| of |
AD
A061801



END
DATE
FILMED
2-79
DDC

12 LEVEL II
NW

NRL Memorandum Report 3874

Failure Studies of a Third Stage Fan Disk From a TF-30 Turbine Engine

W. H. VAUGHAN, R. J. SANFORD, AND J. M. KRAFFT

Ocean Technology Division

W. H. CULLEN

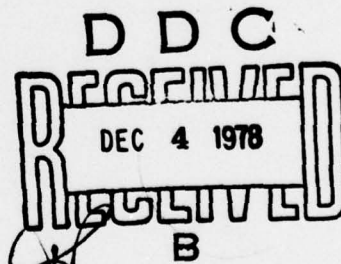
Material Science and Technology Division

and

J. W. DALLY

*University of Maryland
College Park, Maryland 20742*

November 13, 1978



NAVAL RESEARCH LABORATORY
Washington, D.C.

Approved for public release: distribution unlimited.

78 11 30 047

AD A061801

DDC FILE COPY

SECURITY CLASSIFICATION OF THIS PAGE (When Data Entered)

REPORT DOCUMENTATION PAGE		READ INSTRUCTIONS BEFORE COMPLETING FORM
1 REPORT NUMBER NRL Memorandum Report 3874	2 GOVT ACCESSION NO.	3 RECIPIENT'S CATALOG NUMBER
4 TITLE (and Subtitle) FAILURE STUDIES OF A THIRD STAGE FAN DISK FROM A TF-30 TURBINE ENGINE	5 TYPE OF REPORT & PERIOD COVERED Final Report on one phase of a continuing NRL Problem	6 PERFORMING ORG. REPORT NUMBER
		7 AUTHOR(s) W.H. Naughan, R.J. Sanford, J.M. Krafft, W.H. Cullen, and J.W. Dally
8 PERFORMING ORGANIZATION NAME AND ADDRESS Naval Research Laboratory Washington, D. C. 20375	9 CONTRACT OR GRANT NUMBER(s) NRL-MR-3874	10 PROGRAM ELEMENT, PROJECT, TASK AREA & WORK UNIT NUMBERS NRL Problem F01-29 Project A5365.360-0582
11 CONTROLLING OFFICE NAME AND ADDRESS Department of the Navy Naval Air Systems Command Washington, D.C. 20361	12 REPORT DATE November 12, 1978	13 NUMBER OF PAGES 28
14 MONITORING AGENCY NAME & ADDRESS (if different from Controlling Office) 1229 P.	15 SECURITY CLASS (of this report) UNCLASSIFIED	15a DECLASSIFICATION DOWNGRADING SCHEDULE
16 DISTRIBUTION STATEMENT (of this Report) Approved for public release, distribution unlimited.		
17 DISTRIBUTION STATEMENT (of the abstract entered in Block 20, if different from Report)		
18 SUPPLEMENTARY NOTES *University of Maryland College Park, Maryland 20742		DDC RECEIVED DEC 4 1978 B
19 KEY WORDS (Continue on reverse side if necessary and identify by block number) Failure Analysis Turbine Engines		
20 ABSTRACT (Continue on reverse side if necessary and identify by block number) A detailed failure analysis was made of a fan disk from the third stage of the Navy's turbo-jet engine in order to gain a better understanding of the origin and growth kinetics of the cracks that had developed in service. The in service stress that had caused the cracks to originate was determined by a two dimensional photoelastic and holographic stress analysis. A further experimental stress analysis was made to determine the stress intensity factor, after the crack had formed, as a function of crack length. These results were compared with a fractographic study of the bearing surface and the fracture surface. It was found that the striation spacings were in good agreement (Continued)		

DD FORM 1 JAN 73 1473

EDITION OF 1 NOV 65 IS OBSOLETE
S/N 0102-014-8601

SECURITY CLASSIFICATION OF THIS PAGE (When Data Entered)

78 11 30 027
251 950
mt

20. ABSTRACT (Continued)

with the calculated values of the stress intensity factor. Some conclusions were drawn concerning the origin and growth mechanism of these cracks.

DEC 1964
ADVISORY BOARD
PROBATION
B

CONTENTS

INTRODUCTION 1

DISK LUG REMOVAL AND MACROFRACTOGRAPHY 3

MICROFRACTOGRAPHY AND MICROSTRUCTURE 8

STRESS INTENSITY FACTOR DETERMINATION 16

DISCUSSION 21

CONCLUSIONS 22

ACKNOWLEDGMENT 23

REFERENCES 24

ACCESSION FOR

NTIS White Section

DTIC Easy Section

BY _____

SYSTEMS/PROGRAMS/ANALYSIS CODES

Dist. or SPECIAL

A

FAILURE STUDIES OF A THIRD STAGE FAN DISK FROM A TF-30 TURBINE ENGINE

INTRODUCTION

In recent years, the Navy has experienced unusual maintenance problems with its F-14 fighter aircraft. One of these is a tendency to develop cracks in the third stage fan disk of its TF-30 turbo-jet engines. These cracks typically originate in the dovetail region (Fig. 1) near the inner edge of the bearing surfaces between the disk and blades. A fully developed crack viewed from the leading edge of the dovetail is shown in Fig. 2. Cracks developed in this region after an unexpectedly short period of service. An investigation demonstrated a correlation between incidence of cracking and radial clearance between the second- to third-stage air seal. It was found that all of the failures had occurred in engines for which the clearance exceeded 0.025 in. (0.6 mm). This clearance was found to reduce the effective stiffness of the third stage disk, resulting in a strong 2E mode resonance within the operating speed range of the engine ($< 10,500$ rpm). This resonance results in vibratory stresses the order of 15 ksi (103 MPa) which, superposed on the high centrifugal stress, induce high frequency fatigue failures. A program to reduce the air-seal clearance has essentially eliminated this mode of failure and increased the service life of this part. However, fatigue cracking problems were found in other parts of the engine. Thus several studies were initiated at NRL to probe general aspects of the problem.

In fatigue failures, the applied stress and the material resistance to crack formation are of primary importance. To determine the stress, a two-dimensional photoelastic and holographic

Manuscript submitted July 3, 1978.

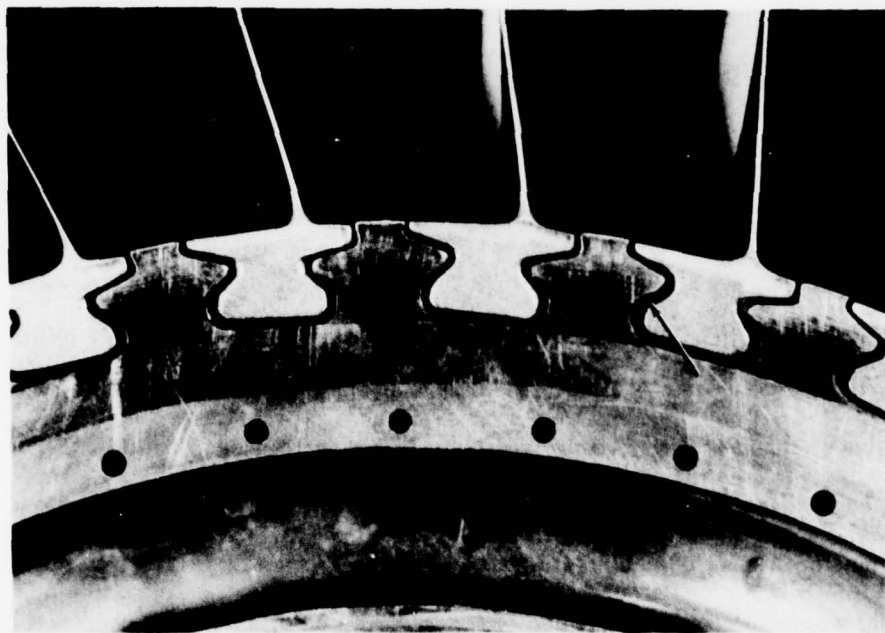


Fig. 1 — Side view of the intact portion of the third stage fan rotor showing the dovetail attachment of the blades. The arrow indicates the region where fretting occurs.



Fig. 2 — Edge view of a fully developed crack. Initially the fracture surface was normal to the fretting surface. It turned into a horizontal plane when it reached the crown of the lug.

analysis was performed for the dovetail region [1]. The results demonstrated that a high stress concentration exists in the fillet and the adjacent bearing area, thus enhancing the probability of initiation of fretting cracks. A finite element analysis of the same region [2] to determine the influence of variations in the distribution of bearing forces indicated similar results.

Concurrently with these mechanics-oriented investigations, a materials study was undertaken to determine if a suitable heat treatment could be developed which would produce a microstructure providing superior resistance to fatigue crack propagation in the titanium alloy (Ti-8Al-1Mo-1V). Previous experience with the alloy Ti-6Al-4V indicated that heat treatments above the beta transition temperature [3] produce a more resistant microstructure. Preliminary results [4] are encouraging with definitive results due soon.

Lastly, a detailed failure analysis of a cracked disk removed from service was performed to determine if features of the fracture surface could be used to discern the failure mechanism. This report describes the results of that study.

This investigation involved an examination of a single third-stage fan disk removed from service after 372 hours of operation. The disk was supplied to NRL by the Naval Air Rework Facility (Norfolk). This disk, which is considered typical of those removed from F-14 aircraft with normal mission profiles, contained a total of 16 observable cracks in 15 of the 36 lugs. Additional cracks which had not penetrated to the end faces of the lugs were uncovered during the course of the study.

DISK LUG REMOVAL AND MACROFRACTOGRAPHY

In order to examine the surface of the cracks which had developed in this disk, it was necessary to separate the cracked lugs by extension of the pre-existent cracks. One possibility

was to saw through most of the remaining section so as to reduce the force for final fracture of the lug; however, this entailed the possibility of damaging the fracture surface. Accordingly a technique was developed which permitted removal of the lugs without sawing. Sufficient force was applied through one dovetail slot to break off an adjacent cracked lug. The blade alone could not be used to apply this force since the thin cross-sectional area would not support the required load. For this reason, the lug portion of a blade (ending at the platform) was joined, by electron beam welding, to a 3.25 in. (82-mm) long titanium shackle having the same cross-section as the platform. This fixture, shown in Fig. 3, sustained forces up to 60 kip (266 kN) (the highest load recorded). The dovetail suffered some damage with each lug failure; the first one had to be replaced after the ninth lug was broken off. In all, fifteen lugs were pulled from the disk by this method. A photograph of the disk mounted in a 100 kip (445 kN) capacity Tinius-Olsen hydraulic testing machine is shown in Fig. 4.

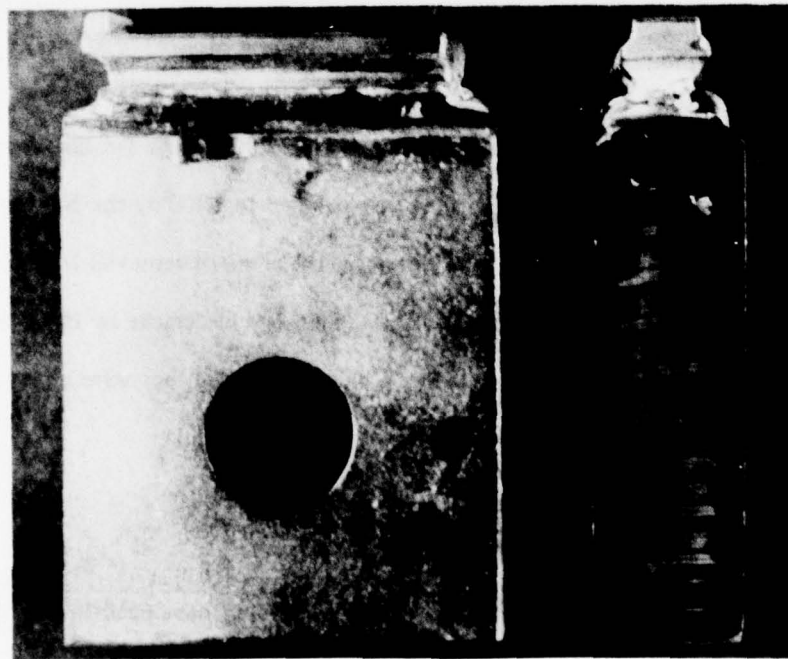


Fig. 3 — The dovetail fixture that was used to pull cracked lugs from the rotor.

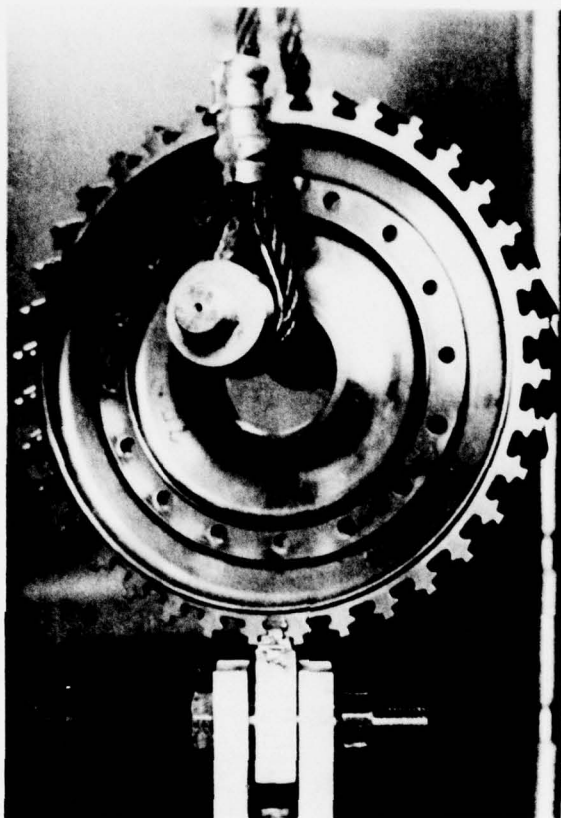


Fig. 4 — The set-up for pulling off cracked lugs in the 100 KIP testing machine

The fracture surface of each of the removed lugs was photographed at 3.25X and examined under a low-power binocular microscope. All of the cracks originated near the inboard edge of the bearing area with the majority (13) of them occurring on the left side of the disk lug (when viewed from the front). The exposed fracture surfaces revealed that the cracks are initially planar and follow the same path as shown on the surface of the lug (see Fig. 2). Four typical fracture surfaces are shown in Fig. 5. In the figure the front face of the disk is on the right and the lug has been rotated so that the fatigue crack is in the plane of photograph. As can be seen, the cracks have quarter-elliptical fronts, of a high length-to-depth ratio, centered

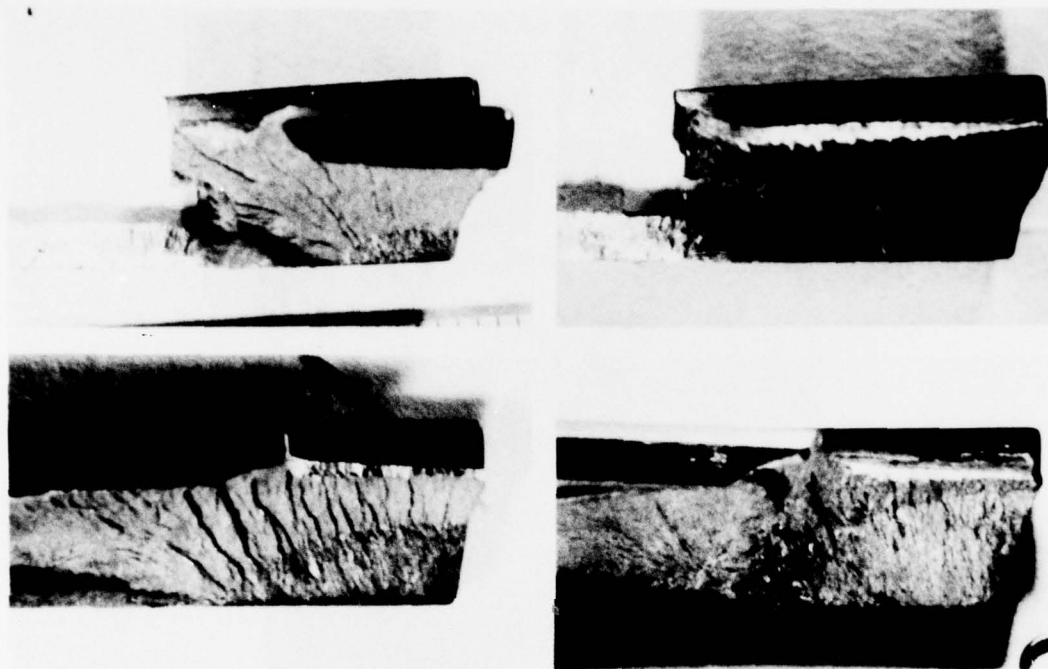


Fig. 5 — Typical cracks that started in the leading edge.

near the slot to front face intersection. The smoothness of the surface texture relative to the fast fracture region beyond the elliptical perimeter suggests that they grew as fatigue cracks, which later high-resolution examination verified. While most of the cracks emanated near the forward leading corner of the disk lug, a small crack (see Fig. 6) was found in the rear of a disk lug. The cracks originated in the fret zone or in the fillet region just below the fret zone. It appears that a given crack initiates at several points over a distance of the order of millimeters along the edge of the slot. This accounts in part for the relatively high ratio of the length of the crack along the disk slot relative to its depth in the lug. The pattern of growth as cracks progress from their origin is relatively consistent, as shown, Fig. 7, in an overlay of this series of various sized cracks.

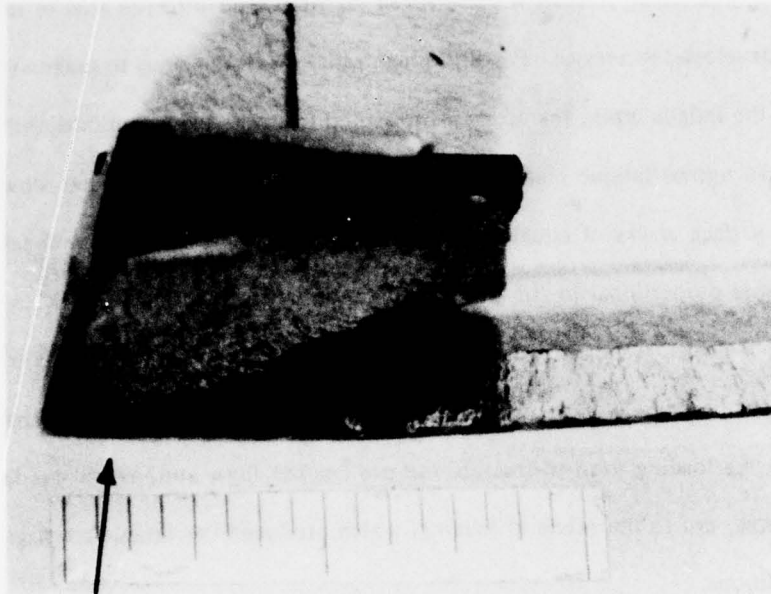


Fig. 6 - A typical crack that started in the trailing edge.

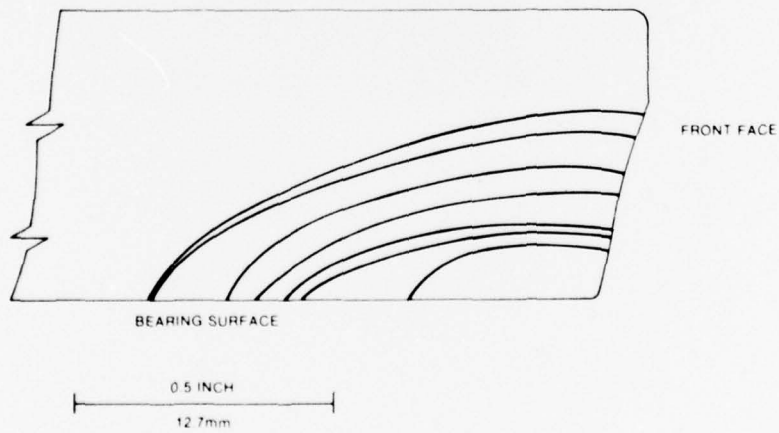


Fig. 7 - Tracings of the leading edge of seven cracks that developed in service. They appear to have a consistent pattern of initiation and growth.

The force required to fracture a pre-cracked lug decreased with the area of the crack surface that had developed in service. For those lugs which fractured so as to make visible the initial surface of the fatigue crack, the area was measured from the low magnification photographs. The failure load versus fatigue crack area is shown in Fig. 8. Irwin [5] has shown that, for semi-elliptical surface cracks of equal aspect ratio, with loading normal to the crack, the stress intensity factor is proportional to the product of the breaking load and the fourth root of the crack area, A . The data used in Fig. 9 shows this dependency when plotted as $\sigma \sqrt[4]{A}$ versus crack area, where σ is the average stress on a lug at failure. It should be noted that this result applies only to the loading used to fracture the pre-cracked lugs, and, as will be demonstrated later in the report, not to the mode of loading, which produced the fatigue crack growth under in-service conditions.

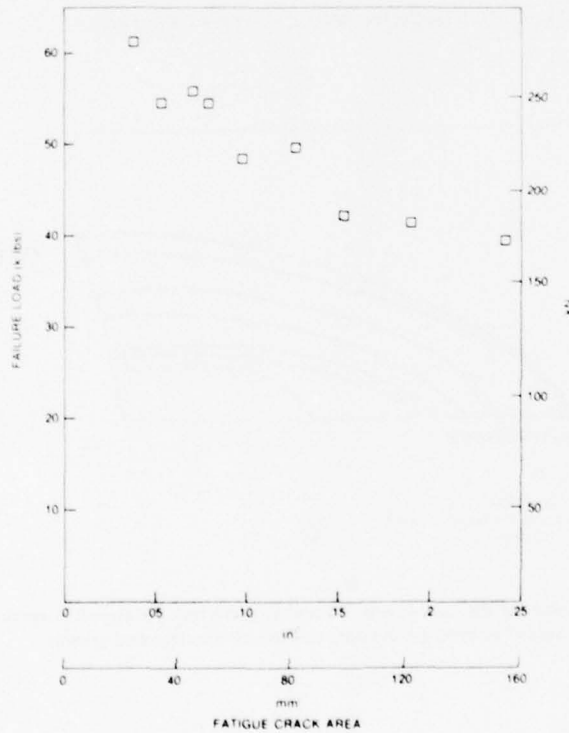


Fig. 8 — The ultimate load to remove a lug as a function of the area of the crack that developed in service.

NRL MEMORANDUM REPORT 3874

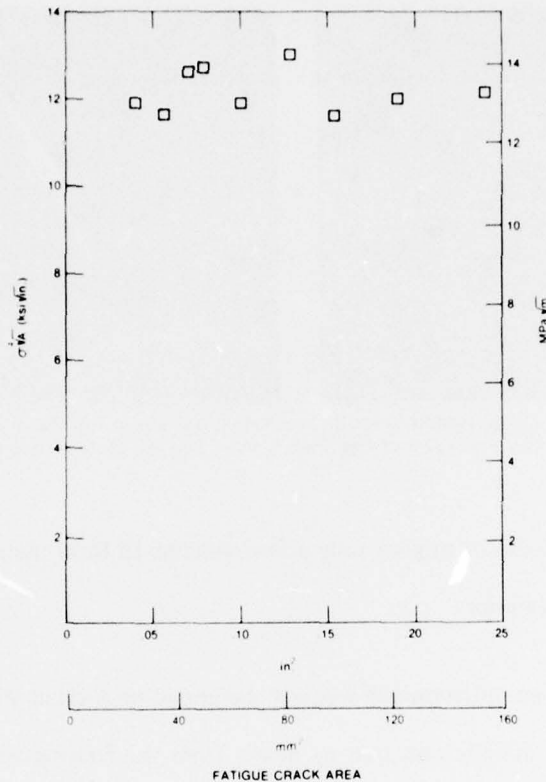


Fig. 9 — This shows that the fourth root of the product of the ultimate load and the crack area is a constant. However this was not the state of stress that occurred in service.

MICROFRACTOGRAPHY AND MICROSTRUCTURE

Fractographic examination included two surfaces: the lug bearing surface for traces of fissures; and the face of the fatigue crack surface accessed by separating the partially cracked lugs. To facilitate access to the fretted surface, two lugs which had developed small cracks in service were removed for microscopic examination by sawing them off across the necks of the lugs while taking care not to disturb the bearing area. Typical SEM pictures of the contact surface around the fret zone Fig. 10, show many potential crack origins which could have started cracks other than the ones that culminated in the observable macrocrack. Although initially

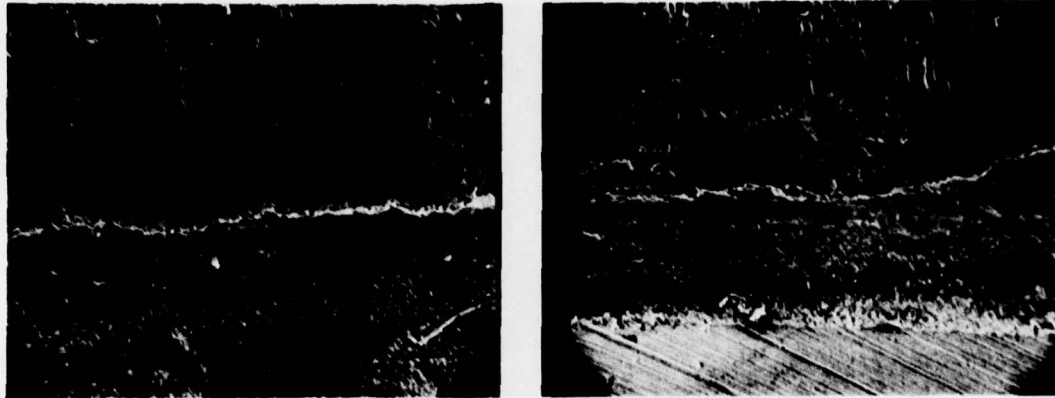


Fig. 10 — SEM micrographs of the fracture trace on the bearing surface in the region where the multiple origins occurred. It can be seen that this is a region of high contact stress and that there is little evidence of abrasion in the vicinity of the crack. (100x)

there is apparently a plethora of origins, only a few combine to form the single dominant crack which advances into the interior.

The region around an initiation site was also examined on a crack which had been broken open. The origins were initially obscured by debris from the fretting which had been forced into the crack and was adhering to the crack surface as illustrated in the upper portion of Fig. 11. This debris was stripped off by repeated application and removal of a polycarbonate replica material. The difference in visibility between an unstripped and stripped fracture origin is seen by comparing Fig. 11 and Fig. 12a. Once the debris was stripped away, it was found that the shape of the grains is not clearly defined near the origin, as shown in Fig. 12b. It is possible that the loss of definition is due to abrasion of the fracture surface by fretting debris or to extensive plastic deformation at the fracture initiation site. It can be seen that the origin of the fracture surface is inclined at an acute angle to the bearing surface unlike the rest of the fracture surface which is essentially perpendicular to the bearing surface. This behavior is typical of fretting origins under the contact zone when shearing forces are present.

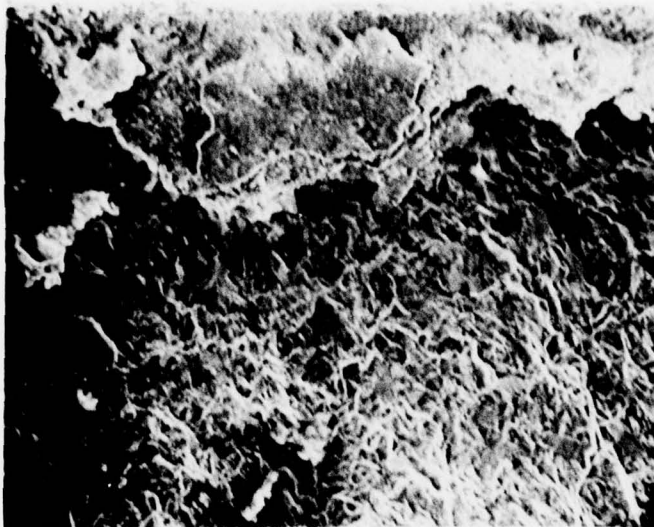


Fig. 11 — SEM micrograph (200x) showing typical fretting debris along the region where the multiple crack origins occurred

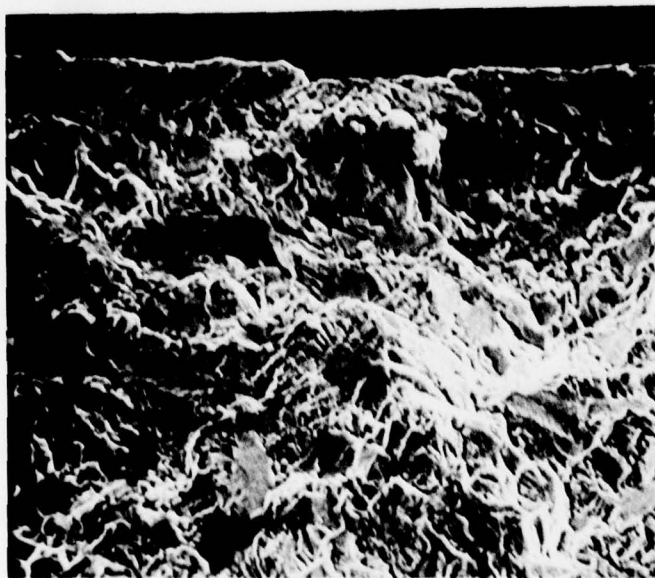


Fig. 12a — SEM micrograph (500x) showing the contrast in microstructure between the cleaned fracture origin at the top and the quasicleavage at the bottom.



Fig. 12b — SEM micrograph (2k x) of the fracture origin shown in 12a

The initial attempt to observe fatigue striations was made in a Cambridge "Stereoscan" electron microscope. The SEM, which requires no replication of the surfaces, was used as the fastest way to examine a large number of locations on the fracture surfaces. However, the SEM photographs would reveal striations only if they were of relatively high contrast. Such striations were found on such a small fraction of the fracture surface that it was necessary to use a method with greater sensitivity. To this end, a standard shadowing technique was used where a replica material was applied to the fracture surface and stripped off to serve as a base for the replica. A dense metallic film was then evaporated on the replica surface at an oblique angle in such a way as to enhance the contrast of any ridges perpendicular to the general direction of fracture propagation. The replicas were then examined in a transmission electron microscope (TEM). It was found that a larger fraction of the fracture surface exhibited evidence of fatigue striations. Even with this method, however, striations were found only in small, widely scattered areas, as is characteristic of titanium alloys.

Figure 13 shows several TEM fractographs taken from various regions of the fatigue crack. It was anticipated that the striation spacings would become larger with distance from the surface, corresponding to the stress intensity factor increasing with crack length. Surprisingly, this was not the case. The striations which were formed all had low contrast and a constant spacing that averaged around $.04 \mu\text{m}$ on the portion of the fracture surface perpendicular to the bearing surface. Only after the fatigue crack turned tangentially across the lug did the striation spacing increase, becoming 2 to 5 times larger. These small striations are barely visible in Fig. 13. There is evidence of groups striations with spacings of the order of $0.5 \mu\text{m}$ (2×10^{-5} in.) in the initial stages of fatigue crack growth, increasing to $1.5 \mu\text{m}$ (6×10^{-5} in.) after the crack turns. These groups are clearly visible in Fig. 13. It is reasonable to associate these group spacings with low cycle engine fluctuations. Thus it appears that high cycle fatigue striations are superposed on low cycle engine fluctuations.

The path of the crack through each lug is not along the direction of maximum tensile stress that develops under centrifugal loading, as indicated by the two-dimensional stress analysis studies of the lug [1, 2]. This analysis would lead one to expect the crack to turn into the tangential direction a short distance from the surface and then to propagate in a direction normal to the direction of maximum tensile stress. One possibility for the observed fracture path is that the cracks are following a line of low fracture toughness resulting from flow patterns produced by the forging operation. To investigate this a cross-section of a lug was polished, etched, and examined in an optical microscope. The micrograph shown in Fig. 14, which was typical of the whole lug, shows that the microstructure is alpha phase in the white areas and acicular alpha plus beta in the dark area. The alpha/beta region showed some signs of an incipient transformation to lamellar alpha-beta. Such microstructure is typical of titanium-



Fig. 13 — Examples of the fatigue striations found at the depths indicated by arrows. These micrographs were made in a TEM from replicas.

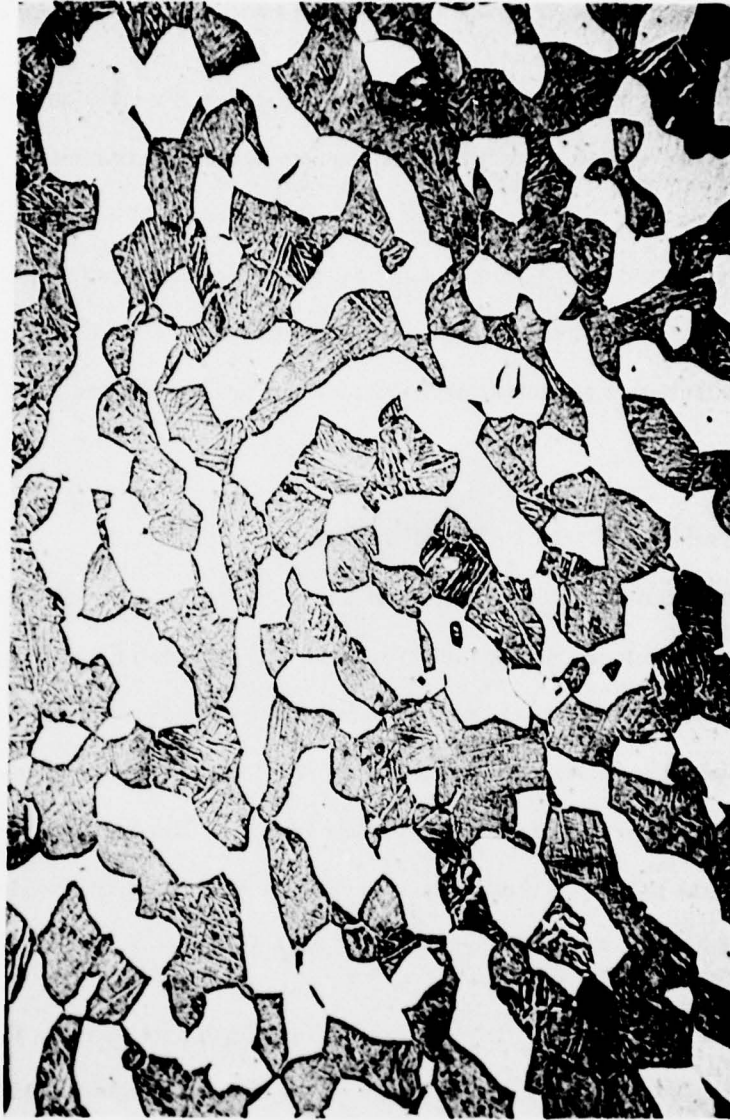


Fig 14 — Microstructure of the third stage fan lug. It is primary alpha in the light areas and acicular alpha plus beta in the dark areas. There is no evidence of a preferred orientation.

aluminum alloys which have been air-cooled from the alpha-beta transition region of the phase diagram. There is no evidence of a pattern of flow lines associated with the forging process.

Another possible indicator of anisotropy in the lug section is a variation in hardness. To check this, a polished section was examined with microhardness measurements along various directions. The values of the micro-hardness level are relatively uniform, indicating no more variation than one would expect from the normal scatter in such measurements. Thus the crack path is not due to anisotropy or flow lines in the lug section. However, texturing of grain orientation, detectable by x-ray diffraction techniques, was not assessed and hence is yet a possibility.

STRESS INTENSITY FACTOR DETERMINATION

In an effort to understand the peculiar path taken by a crack propagating from the bearing surface, a study was made of the stress intensity factor as a function of crack length along this path. One of the photoelastic models that had been used in the earlier work by Parks and Sanford [1] was obtained for study. A simulated crack was formed with a jeweler's saw along a path corresponding to that typically observed in these fractures. The saw crack was extended in small steps along the path of the actual fatigue crack of the disk in service. Isochromatic fringe patterns were recorded for fifteen different values of crack extension.

Typical isochromatic fringe patterns obtained during the test are shown in Fig. 15 with an enlargement of one of these in Fig. 16. Inspection of the fringe pattern of Fig. 16 indicates that the characteristic fringe loops associated with the stress singularity are not symmetric with respect to the crack line and that the fringe loops on either side of the crack line are rotated by different amounts. This configuration of the fringe loops indicates that the driving force on the crack has both opening (K_I) and forward shear (K_{II}) components. The observation that the

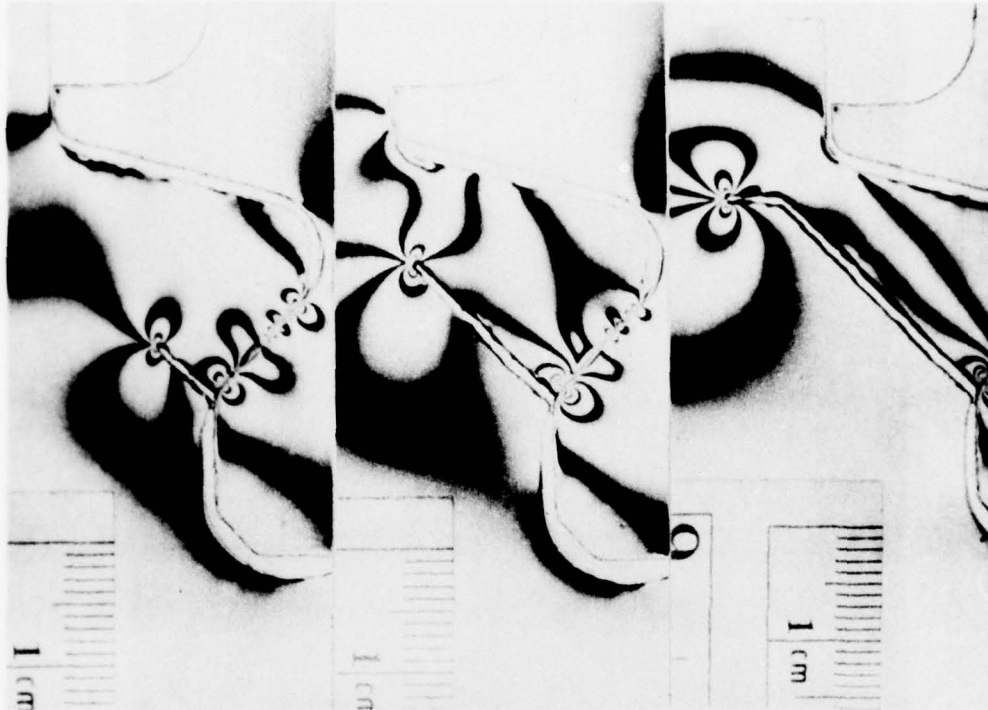


Fig. 15 - Isochromatic fringe patterns of the photoelastic model. They show little change in stress intensity until the simulated crack turned the corner.

fringe loops above and below the crack line are of different size and different rotations indicates that there is an effect due to a non-singular stress component which complicates the analysis.

The relationship between the fringe order, N , with polar coordinates r , θ (relative to the crack tip) and the stress intensity factors, K_I and K_{II} , and an arbitrary non-singular stress, σ_{ox} is given by [6]:

$$\begin{aligned} & \frac{1}{2\pi r} \{ [K_I \sin \theta + 2K_{II} \cos \theta]^2 + [K_{II} \sin \theta]^2 \} \\ & + \frac{2\sigma_{ox}}{\sqrt{2\pi r}} \sin \frac{\theta}{2} [K_I \sin \theta (1 + 2 \cos \theta) + K_2 (1 + 2 \cos^2 \theta + \cos \theta)] \\ & + \sigma_{ox}^2 = (Nf_{\sigma}/h)^2 \end{aligned} \quad (1)$$

where h and f_{σ} are the thickness and optical sensitivity of the photoelastic model, respectively.



Fig. 16 — An enlarged view of the bottom photograph of Fig. 15. The evident asymmetry of the fringe pattern is indicative of the mixed mode state.

Fringe patterns governed by the above relation have received little attention in the literature and no general method for extracting the desired parameters, K_I , K_{II} , and σ_{ox} , from the characteristic features of the fringe loops has been developed. In order to determine these parameters from the fringe patterns of the type shown in Fig. 15 several different methods were

developed and compared for accuracy and sensitivity to small errors. Details of these methods are presented in a separate report [7].

It was concluded in reference [7] that the best method to determine the mixed mode stress intensity factors from photoelastic measurements is to utilize a procedure which matched the fringe order at an arbitrary number of points in the neighborhood of the crack tip to the above-defining equation such that the fitting parameters are the desired unknowns, K_I , K_{II} , and σ_{ox} .

A summary of the values of K_I , K_{II} , and σ_{ox} obtained for the disk are shown in Table I. The values of K_I and K_{II} obtained from the photoelastic model were converted to prototype values by employing the following scaling relationship

$$(K_I)_p = \sqrt{\lambda_1} \lambda_2 \lambda_3 (K_I)_m \quad (2)$$

where λ_1 is the in-plane size scaling factor ($W_m/W_p = 3.409$)

λ_2 is the thickness scaling factor ($h_m/h_p = 0.111$)

λ_3 is the load scaling factor ($P_p/P_m = 24,900/P_m$).

The crack length a is scaled by

$$a_p = a_m/\lambda_1. \quad (3)$$

The tabulated data for K_I and K_{II} associated with the prototype is also given in Table I.

An effective stress intensity factor, K_{eff} , was computed according to the relation

$$K_{eff} = \sqrt{K_I^2 + K_{II}^2} \quad (4)$$

and is shown as a function of crack length in Fig. 17. The results indicate that K_{eff} increases from zero to a maximum value of about 14 ksi $\sqrt{\text{in.}}$ (15.4 MPa $\sqrt{\text{m}}$) as the crack penetrates the region near the fillet with a high stress gradient. The value of K_{eff} remains essentially constant as the crack extends into the lower stress region and propagates across the lug. As the crack

Table I. Summary of Results for K_I , K_{II} and σ_{ox} as a Function of Crack Length for Fan-Blade/Disk

Number of Readings	P Load (lb)	Crack Length (in.)	Model			Prototype			
			K_I (psi $\sqrt{in.}$)	K_{II} (psi $\sqrt{in.}$)	σ_{ox} (psi)	K_I (ksi $\sqrt{in.}$)	K_{II} (ksi $\sqrt{in.}$)	a (in.)	K_{eff} (ksi $\sqrt{in.}$)
Before Crack Turns						Before Crack Turns			
1	800	0.096	573	-569	2482	3.65	-3.63	0.028	5.15
1	1000	0.096	693	-706	2974	3.54	-3.60	0.028	5.05
1	200	0.122	439	-216	327	11.20	-5.51	0.035	12.48
1	200	0.185	475	-159	238	12.12	-4.06	0.054	12.78
5	200	0.241	348	-219	377	8.88	-5.59	0.071	10.49
6	200	0.357	318	-285	357	8.11	-7.27	0.105	10.89
7	200	0.466	512	-203	298	13.06	-5.18	0.137	14.05
7	200	0.622	539	-281	318	13.75	-7.17	0.182	15.51
5	200	0.710	549	-221	134	14.01	-5.64	0.208	15.10
3	200	0.843	392	-334	152	10.00	-8.52	0.247	13.14
5	200	0.955	351	-444	213	8.96	-11.33	0.280	14.44
After Crack Turns						After Crack Turns			
1	200	0.100	793	-365	370	20.23	-9.31	0.29	22.27
3	150	0.190	782	-184	431	26.60	-6.26	0.56	27.33
2	100	0.296	815	-86	131	41.59	-4.39	0.87	41.82
1	100	0.296	786	-163	154	40.11	-8.31	0.87	40.96
1	100	0.410	1044	244	-326	53.28	12.45	1.20	54.71
1	100	0.518	1196	347	-519	61.03	17.70	1.51	63.54

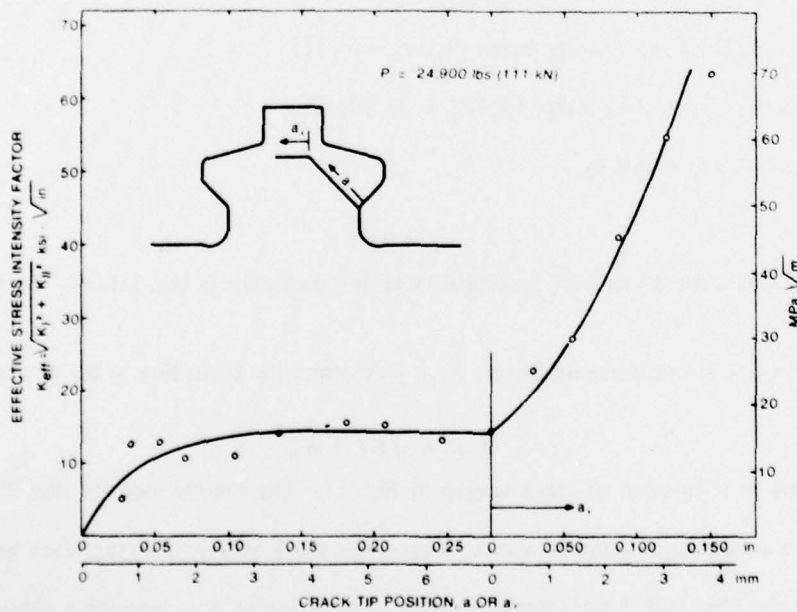


Fig. 17 - The effective crack tip stress intensity factor K_I as a function of the position of the crack tip.

approaches the compressive fillet, K_{II} increases and K_I decreases (see Table 1) until the crack turns through an angle of 45 degrees and begins to propagate circumferentially. At this point K_I increases markedly and K_{II} decreases. With further increases in crack length K_{eff} increases to a value exceeding $60 \text{ ksi } \sqrt{\text{in.}}$ ($66 \text{ MPa } \sqrt{\text{m}}$).

DISCUSSION

The definiteness of this investigation would have been enhanced considerably had the actual flight history and load profile of this disk been known. Even so, certain general observations can be made and a possible mechanism proposed.

By comparing the photoelastically determined stress intensity factor with the observed striation spacing in the region of constant crack growth rate, several conclusions can be drawn concerning loading conditions during crack growth. If one assumes, contrary to the fractographic evidence that the loading was that of low cycle fatigue associated with engine speed fluctuations, the measured stress intensity of $14 \text{ ksi } \sqrt{\text{in.}}$ ($15.4 \text{ MPa } \sqrt{\text{m}}$) at the maximum operating speed of 10,500 rpm would correspond to the upper bound on ΔK , i.e., K_{max} . Assuming large engine speed excursions of 50% or greater ($R \geq .5$), the ΔK would vary between 7-14 $\text{ksi } \sqrt{\text{in.}}$ ($7.7\text{-}15.4 \text{ MPa } \sqrt{\text{m}}$). From the data of Bucci and Paris [8] this range of ΔK would correspond to crack growth rates of the order of 10^{-6} to 10^{-5} in./cycle ($\approx 10^{-7}$ mm/cycle). An examination of the fatigue crack fractography as shown in Fig. 12a, shows this region to consist predominantly of cleavage leaves with little dimple rupture. Yuen et al. [9] have shown that in titanium alloys cleavage is not produced at crack growth rates in the range of 10^{-5} in./cycle or faster. Therefore low cycle fatigue as the primary mechanism of crack growth must be ruled out. The presence of groups of striations as seen in Fig. 13 (upper left) is consistent with the

superposition of high cycle fatigue on the low cycle engine fluctuations through some resonance range.

Considering the possibility of high cycle fatigue, the measured K_{eff} value of $14 \text{ ksi } \sqrt{\text{in.}}$ ($15.4 \text{ MPa} \sqrt{\text{M}}$) would correspond to the mean value and, assuming an R value of 0.95 (small amplitude vibrations), ΔK becomes $0.72 \text{ ksi } \sqrt{\text{in.}}$. Using this value of ΔK in the modified Forman equation given by Bucci and Paris [8] results in an extrapolated crack growth rate of $5.5 \times 10^{-9} \text{ in./cycle}$ ($1.4 \times 10^{-4} \mu\text{m/cycle}$). Assuming this crack growth rate is constant over the region of initial crack growth predicts that the total number of cycles to failure is of the order of 10^8 . This prediction is consistent with the assumption of low amplitude vibratory stresses at the fundamental frequency (governed by the rotational speed) present over a propagation times of 200 hours (i.e., $10,500 \text{ rpm} \times 60 \text{ m/hr} \times 200 \text{ hour} \sim 10^8 \text{ cycles}$). The crack growth rate predicted by this model is of the order of atomic dimensions and accordingly no direct measurement with a TEM of striation spacing can be used to confirm these extremely low crack growth rates. If this explanation is, in fact, the correct picture for the failure of the third stage disk, the solution to the premature failure problem is to increase the crack initiation time by reducing the stress concentrations and/or increasing the resistance to fatigue crack initiation and propagation by material modification.

CONCLUSIONS

Based on the results of the various mechanical tests and fractography performed on the disk, several conclusions can be drawn:

(a) Striation spacings indicate that fatigue crack growth proceeded at a relatively constant rate per cycle over the initial region of crack growth. A photoelastic analysis indicates a constant effective stress intensity factor in the initial region that is consistent with this observation.

NRL MEMORANDUM REPORT 3874

(b) Although the majority of the cracks formed near the leading edge of the lug a small number were found to start at the trailing edge.

(c) SEM studies of the bearing surface indicated the presence of multiple nucleation sites the coalescence of some of which resulted in formation of the dominant macrocrack. The large length to depth ratio of the crack is consistent with this observation. These multiple crack origins were caused by severe stress concentrations associated with the contact stress condition.

ACKNOWLEDGMENT

The results contained in this report were materially helped by Mr. Cedric Beachem, Mr. Dale Meyn and Mrs. Jean DeVault. They provided free access to their facilities and shared their expertise in fractography in a way that made it possible to work much more effectively.

REFERENCES

1. Parks, V.J. and Sanford, R.J. "Experimental Stress Analysis of the TF-30 Turbine Engine Third-Stage Fan Blade/Disk Dovetail Region," NRL Report 8149, August 26, 1977.
2. Beaubien, L.A., "Numerical Parametric Stress Analysis of the TF-30 Turbine Engine Third-Stage Fan Blade/Disk Dovetail Region," NRL Memo. Report 3671, January 1978.
3. Yoder, G.R., Cooley, L.A. and Crooker T.W., "Observations on Microstructurally Sensitive Fatigue Crack Growth in a Widmanstatten Ti-6Al-4V Alloy," *Met. Trans. 8A*, pp. 1737-43, 1977.
4. Yoder, G.R., Cooley, L.A., Crooker, T.W., "Enhancement of Fatigue Crack Propagation Resistance in Ti-8Al-1Mo-1V Through Microstructural Modification," Report of NRL Progress, December 1977, p. 10-11.
5. Irwin, G.R., "Crack-Extension Force for a Part-Through Crack in a Plate," *J. of Applied Mechanics*, Vol. 29, December 1962, pp. 651-654.
6. Paris, P.C. and Sih, G.C., "Stress Analysis of Cracks," *Fracture Toughness Testing and its Applications*, STP 381, American Society for Testing and Materials, Philadelphia, Pa. 1965, pp. 30-81.
7. Sanford, R.J. and Dally, J.W., "Stress Intensity Factors in the Third Stage Fan Disk of the TF-30 Turbine Engine," NRL Report 8202, May 1978.
8. Bucci, R.J. and Paris, P.C., "Fatigue Behavior of a Titanium 8Al-1Mo-1V Alloy in a Dry Argon Environment," *J. of Materials*, Vol. 7, No. 3, September 1972, pp. 402-409.

NRL MEMORANDUM REPORT 3874

9. Yuen, A., Hopkins, S.W., Leverant, G.H. and Rau, C.A., "Correlations Between Fracture Surface Appearance and Fracture Mechanics Parameters for Stage II Fatigue Crack Propagation in Ti-6Al-4V," *Met. Trans.*, 5, p. 1833-42, (1974).